CLIMATOLOGY

Loss of Earth system resilience during early Eocene transient global warming events

Shruti Setty[1]*, Margot J. Cramwinckel[2], Egbert H. van Nes[1], Ingrid A. van de Leemput[1], Henk A. Dijkstra[3,4], Lucas J Lourens[2], Marten Scheffer[1], Appy Sluijs[2]

Superimposed on long-term late Paleocene–early Eocene warming (~59 to 52 million years ago), Earth's climate experienced a series of abrupt perturbations, characterized by massive carbon input into the ocean-atmosphere system and global warming. Here, we examine the three most punctuated events of this period, the Paleocene-Eocene Thermal Maximum and Eocene Thermal Maximum 2 and 3, to probe whether they were initiated by climate-driven carbon cycle tipping points. Specifically, we analyze the dynamics of climate and carbon cycle indicators acquired from marine sediments to detect changes in Earth system resilience and to identify positive feedbacks. Our analyses suggest a loss of Earth system resilience toward all three events. Moreover, dynamic convergent cross mapping reveals intensifying coupling between the carbon cycle and climate during the long-term warming trend, supporting increasingly dominant climate forcing of carbon cycle dynamics during the Early Eocene Climatic Optimum when these recurrent global warming events became more frequent.

INTRODUCTION

As anthropogenic carbon dioxide emissions continue, ongoing global warming might strengthen positive feedbacks that can propel abrupt change in sensitive components of the Earth system (*1*). Particularly important is the possibility of rapid discharge from excitable carbon reservoirs, further exacerbating future global warming. The exchange of carbon between reservoirs and the functioning of the global carbon cycle are strongly time scale dependent (Fig. 1). On geologically short time scales of up to tens of thousands of years, carbon moves through the global exogenic cycle of the ocean, atmosphere, biosphere, surface sediments, and soils. The cycling of carbon on time scales of several hundreds of thousands of years and longer includes exchange between the aforementioned exogenic reservoirs and the rock reservoir through volcanism and carbon burial (*2*). The processes operating on these different time scales can interlink, as slow-storage reservoirs, termed carbon capacitors or tipping elements (Fig. 1), may abruptly release carbon in response to a faster climate forcing, only to be recharged on much longer time scales (*3*, *4*). Such self-enforcing carbon cycle feedbacks include permafrost thawing in response to climate change that may trigger biochemical heat release, thereby propelling the thaw further (*5*). Other reservoirs that might release carbon abruptly include submarine methane hydrates (*6*) and peatlands (*7*). In turn, abrupt changes in one of these reservoirs might trigger a response in others through so-called tipping cascades (*8*, *9*). Constraining the direction and strength of these feedbacks is crucial for adequate climate projections and adaptations, not only for the next century but also for the generations living in centuries and millennia to come (*10*).

The geological record contains Earth's climate history and is our most important test bed to quantify climate-carbon cycle interactions on time scales longer than the reach of observations. During the Cenozoic era [66 million years (Ma) ago to present], the highest-amplitude coupled carbon cycle-climate variations were the transient global warming and carbon cycle disruptions during the late Paleocene–early Eocene (~60 to 50 Ma ago), which are informally termed "hyperthermal events" or "hyperthermals." The onset of the hyperthermals marks rapid climate warming and massive carbon injection into the global exogenic reservoir (Fig. 1) from a still-debated source, and these events are depicted by severe ocean acidification and by large negative excursions in stable carbon isotope ratios ($\delta^{13}C$) in sedimentary sequences (*11*–*14*). Most, if not all, hyperthermal events were paced by changes in (regional) solar insolation through Earth's orbital cycles, notably the eccentricity metronome of Earth's orbit around the sun (*14*–*16*). These orbital cycles drive only minimal changes in the radiative forcing, implying an important role for amplifying feedbacks, especially processes in the exogenic carbon cycle. Moreover, the superposition of hyperthermal events on long-term multimillion year changes in the carbon cycle and climate suggests a link between slow storage and fast release of carbon (*4*, *17*, *18*). Indicators for anomalous changes such as warming (*19*, *20*) and carbon cycle change (*21*, *22*), just before the carbon isotope excursion of the Paleocene-Eocene Thermal Maximum (PETM), have built a strong suspicion that positive carbon cycle feedbacks were involved in amplifying the initial warming leading to this event. Although carbon release from peat and soil organic carbon (*23*), permafrost (*24*), and/or submarine methane hydrates (*3*) have been proposed as possible sources, evidence for carbon input from any of these reservoirs is lacking. Accumulating evidence suggests that volcanic carbon emissions were important during the PETM (*21*, *25*–*27*). The crucial difference between these carbon sources is that volcanic emissions are largely decoupled from processes on Earth's surface, while the catastrophic release of carbon from potential carbon capacitors may be governed by climate and, thus, orbital cycles and associated feedbacks (Fig. 1). Therefore, beyond the identification of the specific

[1]Department of Environmental Science, Wageningen University and Research, Droevendaalsesteeg 3a, 6708 PB Wageningen, Netherlands. [2]Department of Earth Sciences, Faculty of Geoscience, Utrecht University, Princetonlaan 8a, 3584 CB Utrecht, Netherlands. [3]Institute for Marine and Atmospheric research Utrecht, Department of Physics, Utrecht University, Princetonlaan 5, 3584 CC Utrecht, Netherlands. [4]Centre for Complex Systems Studies, Utrecht University, Princetonlaan 5, 3584 CC Utrecht, Netherlands.
*Corresponding author. Email: shruti.setty@wur.nl

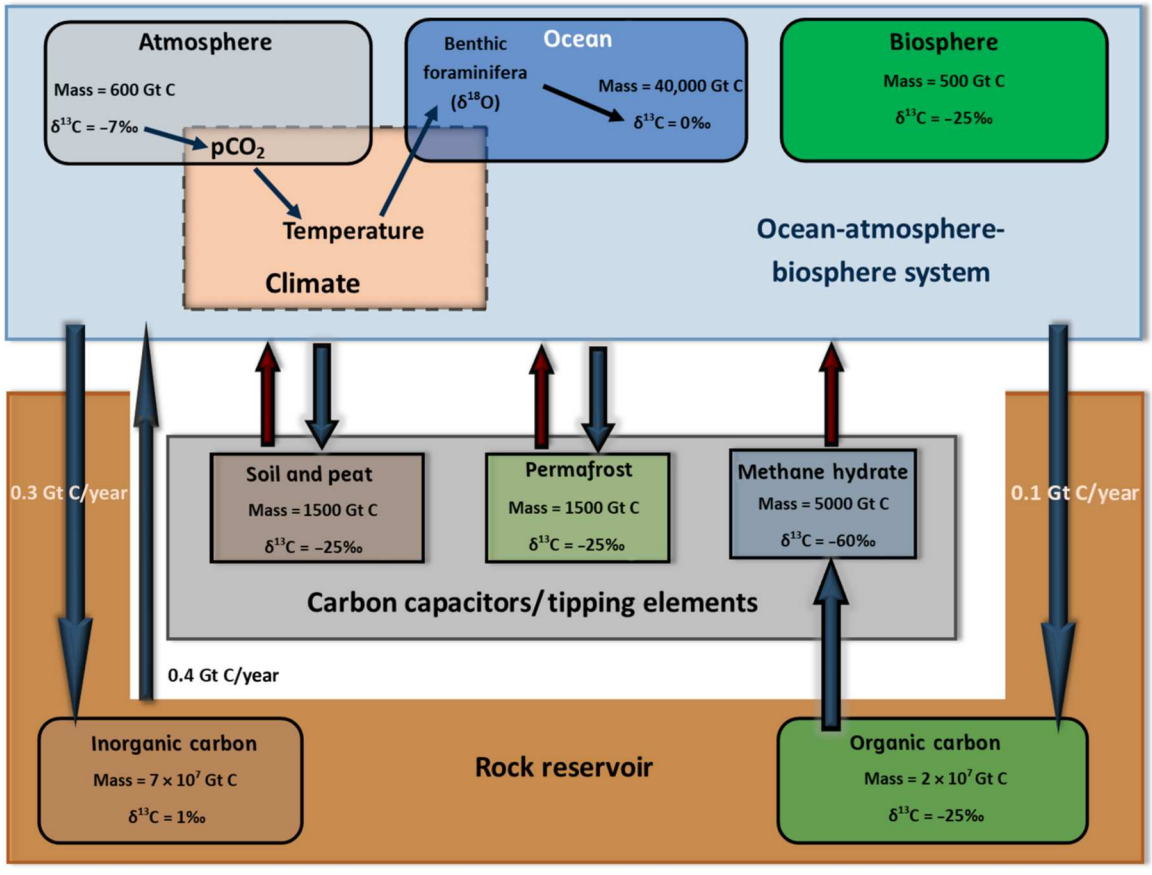

Fig. 1. Schematic representation of interactions between ocean-atmosphere-biosphere system and rock reservoir with potential carbon capacitors/tipping elements. Here, benthic foraminifer $\delta^{13}C$ and $\delta^{18}O$ records are used as tracers of carbon cycling and climate, respectively (see text). Storage of carbon in the carbon capacitors/tipping elements occurs slowly over tens to hundreds of thousands of years (blue arrows), while release of carbon may be fast and abrupt within millennia (red arrows) upon perturbation.

carbon source, the central question is whether these hyperthermal events were mainly externally forced (e.g., by volcanic emissions) or internally driven by positive feedbacks within the coupled climate-carbon cycle system, resulting in an amplified response to small orbitally paced climate variation.

Late Paleocene–early Eocene climate and carbon cycle variability can be assessed from an 18.3-Ma-long dataset of paired deep ocean benthic foraminiferal oxygen ($\delta^{18}O$) and stable carbon isotope ($\delta^{13}C$) ratios from the South Atlantic Ocean (Figs. 1 and 2, A and B) (*16*, *28*). These records are of high resolution (1.5 to 4 ka) and are stratigraphically complete, with a well-resolved age model. The variability in the $\delta^{18}O$ record dominantly reflects deep ocean temperature variability as continental ice sheets were largely absent. In turn, deep ocean temperature variability relates strongly to the global average temperature, which was governed by the atmospheric CO_2 concentrations and associated feedbacks (*29*, *30*). The variability in the $\delta^{13}C$ record reflects the $\delta^{13}C$ signature of the dissolved inorganic carbon (DIC) of the deep ocean ($\delta^{13}C$-DIC), which is the dominant reservoir in the global exogenic carbon pool (Fig. 1). On time scales of up to 10^4 years, it reflects the redistribution of carbon with different $\delta^{13}C$ values, notably resulting from organic matter production and processing, between oceanic, atmospheric, biogenic, and surficial sediment (soils and sea floors) reservoirs (*31*). On time scales of up to 10^5 years, carbon with distinctly low $\delta^{13}C$ values (^{13}C-depleted) may also be stored in peat and methane hydrates, leaving the oceanic DIC with high $\delta^{13}C$ values (^{13}C-enriched) (*4*). The negative carbon isotope excursions observed across hyperthermal events have been related to massive carbon release from such reservoirs (Fig. 1) (*3*, *20*). On even longer, multimillion year time scales, whole-ocean $\delta^{13}C$-DIC is controlled by the burial of ^{13}C-depleted organic carbon relative to ^{13}C-enriched carbonate in the rock reservoir (*2*) and possibly by methane hydrate dynamics (*17*).

In this study, we target the deep ocean benthic foraminifer $\delta^{18}O$ and $\delta^{13}C$ records for climate and carbon cycle variability, respectively, to constrain the strength of external drivers versus internal carbon cycle feedbacks and Earth system resilience using mathematical approaches based on the theory of dynamical systems. Loss of resilience is an attribute displayed by complex systems with alternative stable states, such as the Earth system, as changing conditions cause them to approach a "tipping point". More specifically, in the vicinity of the classical tipping point, e.g., a saddle-node bifurcation, the return rate to the equilibrium or the stable state upon small perturbations becomes very slow, a phenomenon known as critical slowing down [see, e.g., (*32*, *33*)]. In natural time series, this can be reflected in an elevated temporal autocorrelation

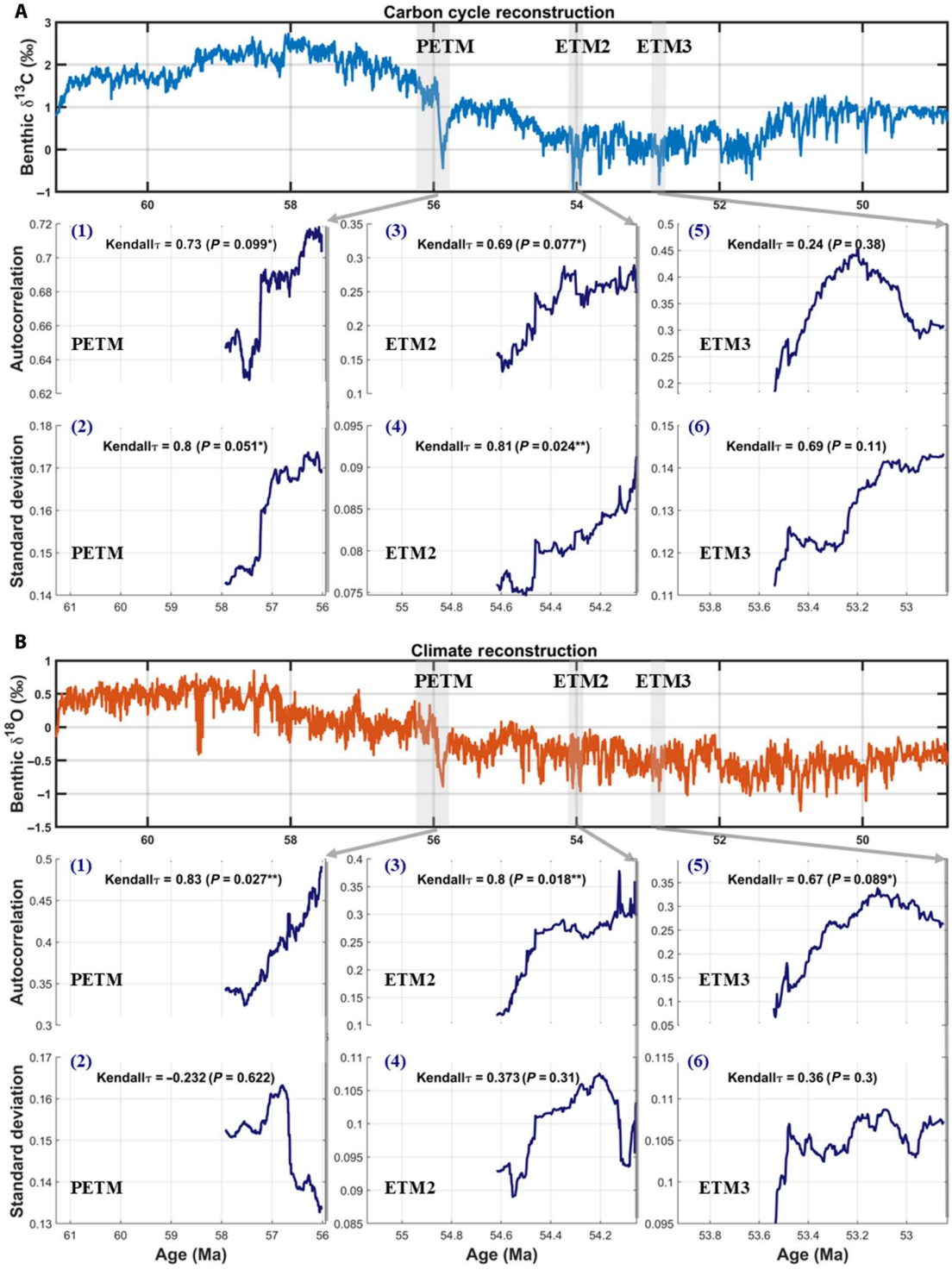

Fig. 2. DIORs before the three global warming events. Sliding window DIORs analysis of the paired benthic $\delta^{13}C$ and $\delta^{18}O$ isotope ratios between 61.28 and 48.8 Ma. (**A**) $\delta^{13}C$ record. (**B**) $\delta^{18}O$ record. (A) Sliding window autocorrelation indicator before PETM (1), ETM2 (3), and ETM3 (5) in the $\delta^{13}C$ record. (A) Sliding window SD indicator before PETM (2), ETM2 (4), and ETM3 (6) in the $\delta^{13}C$ record. (B) Sliding window autocorrelation indicator before PETM (1), ETM2 (3), and ETM3 (5) in the $\delta^{18}O$ record. (B) Sliding window SD indicator before PETM (2), ETM2 (4), and ETM3 (6) in the $\delta^{18}O$ record. For all the three events, the size of the sliding window taken was 50% of the curated dataset (PETM: 699 data points, 2.6715 Ma; ETM2: 208 data points, 540.5 ka; ETM3: 206 data points, 533 ka), and the bandwidth used for Gaussian detrending removed variability over ca. 500 ka for PETM and ca. 30 ka for ETM2 and ETM3.

and standard deviation (SD), hereafter referred to as dynamical indicators of resilience (DIORs). In generic terms, the mechanism causing the loss of resilience in the vicinity of a tipping point is a strengthening positive feedback compared to the stabilizing negative feedbacks (*33*, *34*). We assess changes in resilience over geological time by computing DIORs before the three most prominent hyperthermal events, the PETM and the Eocene Thermal Maximum 2 and 3 (ETM2 and ETM3) (*35*–*38*) using a sliding window. Furthermore, we use convergent cross mapping (CCM) to infer the strength of the interactions between the climate and the carbon cycle as reflected in the $\delta^{18}O$ and $\delta^{13}C$ records. CCM is a nonlinear attractor reconstruction–based method that tests for causal interaction between different variables in a dynamical system and can distinguish between the directions of causation (*39*, *40*). The CCM method has been successfully applied to study Earth system feedbacks during the more recent glacial-interglacial cycles (*41*, *42*). To assess how the strength of feedbacks may change over time, we use it in a sliding window and name this approach Dynamic Convergent Cross Mapping (DCCM). Moreover, to assess the robustness of the DCCM analysis, we did a similar analysis using another causality detection method based on machine learning. This reservoir computing causality (RCC) method uses an echo state neural network for predictions (*43*). The sliding window approach of this analysis is named as dynamic reservoir computing causality (DRCC) (see Materials and Methods).

RESULTS AND DISCUSSION

Loss of Earth system resilience toward the hyperthermal events

A significant rise in autocorrelation and SD occurs toward most hyperthermal events (Table 1 and Fig. 2). Before both the PETM and ETM2, there is an increase in both autocorrelation and SD in the $\delta^{13}C$ record, and there is also an increase in the autocorrelation trend of the $\delta^{18}O$ records (all within 90% confidence level). In the DIORs leading to ETM3, the trends in autocorrelation and SD are overall positive. These trends are, however, less strong than those before the PETM and ETM2, except the autocorrelation indicator in the $\delta^{18}O$ record, which is within the 90% confidence level. This may be related to a lower amplitude of the ETM3 event in combination with stronger background variability (that is, lower signal-to-noise ratio). These results are not sensitive to the choice of window size, bandwidths, and interpolation method as shown in text S1 and figs. S1 to S4.

Our results showing slowing down before the three hyperthermals are consistent with previous studies suggesting the loss of Earth system resilience preceding PETM (*44*, *45*). The fact that we find similar behavior of dynamic indicators of resilience preceding the PETM, ETM2, and ETM3 suggests a common mechanistic origin for all these global warming events, as part of a characteristic Earth system response. The critical slowing down could perhaps be in relation to the weakening of the oceanic overturning circulation in response to orbital change before hyperthermal events (*18*, *46*, *47*). In addition, in the ice-free Eocene, reinforcing carbon cycle feedbacks in response to small initial cyclic orbital forcing (eccentricity and precession) have also been pinpointed as a likely systematic response (*29*, *46*, *47*). Such feedback mechanisms might have led to the interpreted loss of Earth system resilience. This may imply that the large input of volcanic carbon during the PETM was temporally coincidental, perhaps contributing to the large magnitude and duration of the PETM relative to the other hyperthermals (*21*, *25*).

Table 1. Rolling window dynamic indicators of resilience for the three global warming events.

System	Autocorrelation		SD	
	Kendall-τ	*P* value	Kendall-τ	*P* value
Paleocene-Eocene Thermal Maximum (PETM)				
Carbon cycle	0.732	0.099*	0.795	0.051*
Climate	0.829	0.027**	−0.232	0.622
Eocene Thermal Maximum 2 (ETM2)				
Carbon cycle	0.686	0.077*	0.806	0.024**
Climate	0.799	0.018**	0.373	0.306
Eocene Thermal Maximum 3 (ETM3)				
Carbon cycle	0.237	0.379	0.694	0.106
Climate	0.671	0.089*	0.359	0.297

*P < 90% confidence interval. **P < 95% confidence interval for Kendall-τ.

DCCM and the Eocene hyperthermals

To further investigate the origin of the inferred loss of resilience leading up to the hyperthermal events, we here introduce DCCM, an adapted moving-window CCM method to examine the dynamic causal interaction, i.e., causality, between the global carbon cycle ($\delta^{13}C$) and the climate ($\delta^{18}O$). We address the causal effect (given by CCM skill) of the carbon cycle dynamics on the climate, i.e., "CCM skill of $\delta^{13}C$ on $\delta^{18}O$" as $\delta^{13}C \rightarrow \delta^{18}O$, and climate on the carbon cycle dynamics, i.e., "CCM skill of $\delta^{18}O$ on $\delta^{13}C$" as $\delta^{18}O \rightarrow \delta^{13}C$. We surmise that, as the global carbon cycle approaches a tipping point, $\delta^{13}C \rightarrow \delta^{18}O$ increases because of the strengthening of the positive feedback between the connected carbon cycle system and climate system [see also (*48*)]. This, in turn, could have resulted in the amplification of bidirectional feedbacks simultaneously pushing the climate toward a transition (*49*).

As depicted in Fig. 3C, the DCCM analysis hints at a generally high synchronization between the carbon cycle and climate during the early Eocene (56 to 48 Ma ago), represented by high CCM skills averaging over 0.7 (within the 95% confidence level). In addition, periods such as the Paleocene Carbon Isotope Maximum (PCIM) and hyperthermal events such as the PETM and ETM2 stand out as anchors of fluctuating causal interactions between the climate and carbon cycle. The DCCM analysis points toward an amplification of internal feedbacks before the PETM and ETM2. During the PETM and ETM2 itself, both $\delta^{13}C \rightarrow \delta^{18}O$ and $\delta^{18}O \rightarrow \delta^{13}C$ showed wed potential causal effects. Although it seems that $\delta^{18}O \rightarrow \delta^{13}C$ was stronger than $\delta^{13}C \rightarrow \delta^{18}O$, suggesting that Earth system seems toward being more climate-driven, this difference is unlikely to be significant because of bidirectionality.

Along with the DCCM analysis, we performed two important tests in the curated datasets, namely, a convergence test and a test using extended CCM (ECCM) to examine whether the causal interaction was not observed because of spurious correlation or a

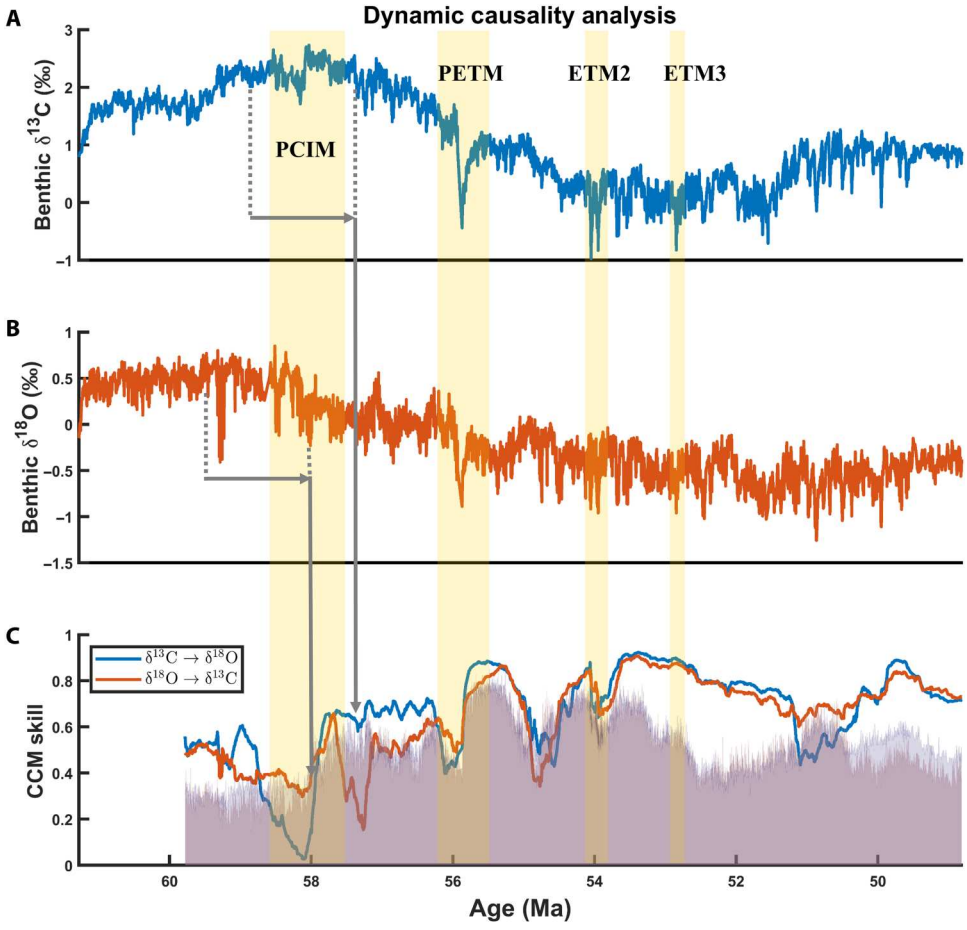

Fig. 3. DCCM analysis between the paired benthic $\delta^{13}C$ and $\delta^{18}O$ isotope ratios during the late Paleocene and the early Eocene from the Walvis Ridge in the South Atlantic Ocean. (**A**) Benthic $\delta^{13}C$ isotope ratios representing the carbon cycle reconstruction. (**B**) Benthic $\delta^{18}O$ isotope ratios representing the climate reconstruction. (**C**) DCCM analysis. The CCM skill of the effect of the carbon cycle dynamics on climate, addressed as $\delta^{13}C \rightarrow \delta^{18}O$, and the CCM skill of the effect of the climate on carbon cycle dynamics, addressed as $\delta^{18}O \rightarrow \delta^{13}C$. The CCM skills were calculated using a moving window of 350 data points (~1 Ma) and a library size of 349 data points; embedding parameters of time lag-τ = 4, and embedding dimension, E = 6. The light blue– and red-colored regions depict the CCM skill within the 95% confidence interval of $\delta^{13}C \rightarrow \delta^{18}O$ and $\delta^{18}O \rightarrow \delta^{13}C$, respectively, using 100 surrogate null models generated by the power spectrum method.

common driver of both the systems, respectively (see Materials and Methods for more details). To simplify these analyses, we tested this just before PCIM, the three hyperthermals, and after ETM3 (see Table 2, "Studied time ranges"). In these five intervals, the convergence tests were positive for causality, and displayed that the causal interactions were bidirectional before PCIM, PETM, ETM2, ETM3, and after ETM3 (fig. S5). The convergence test depicted that the CCM skills keep increasing as the climate-carbon cycle system moved from PCIM toward ETM3, after which the CCM skills starts decreasing again. Furthermore, the ECCM analysis exhibited remarkably clearly that the high synchronization observed during the early Eocene implies a strong intrinsic causal interaction between the climate and the carbon cycle dynamics, which are not necessarily the sole effect of the eccentricity metronome (fig. S6). ECCM analysis indicated that $\delta^{13}C \rightarrow \delta^{18}O$ in the curated dataset for PCIM does not represent a causal relationship, as the maximum CCM skills are found for future time difference. This is an indication that, in this period, the causal relation between $\delta^{13}C$ and $\delta^{18}O$ is not bidirectional but that the causal relationship is due to a common driver of both the systems (*50*).

Early Eocene increase in system sensitivity to perturbation

In the oldest part of the analyzed record, $\delta^{13}C \rightarrow \delta^{18}O$ decreases, culminating in the lowest recorded CCM skill toward the PCIM (Fig. 3). Here, $\delta^{18}O \rightarrow \delta^{13}C$ was also minimal, although it is not completely insignificant. During the PCIM, $\delta^{13}C \rightarrow \delta^{18}O$ is exceptionally low and is not indicating a causal relationship, which is interesting as the PCIM has been related to massive storage of ^{12}C-rich organic carbon out of the exogenic carbon pool (*49*). During this time, carbon cycle fluxes relevant to forcing climate apparently were more dominated by the inorganic carbon cycle and, thus, were leaving less of an imprint on the benthic $\delta^{13}C$ record. Right after the PCIM, $\delta^{13}C \rightarrow \delta^{18}O$ begins to increase and generally continues to rise across the long-term decrease in $\delta^{13}C$ values until ~53 Ma ago. A similar positive trend marks $\delta^{18}O \rightarrow \delta^{13}C$ between the late Paleocene and the early Eocene (up to ~53 Ma ago). Both $\delta^{13}C \rightarrow \delta^{18}O$ and $\delta^{18}O \rightarrow \delta^{13}C$ show remarkably high values (0.7 to 0.9; within 95% confidence level) and almost identical trends throughout most of the early Eocene. Especially, the period between 54 and 51 Ma ago, which culminates in the Early Eocene Climatic Optimum (EECO) (*16*, *51*), has a consistently high and

Table 2. Convergence test of the curated data. Here, the converging CCM skill at a library size of 350 data points in the time range preceding different periods (PCIM and after ETM3) and the three abrupt events are given (for uniformity). The CCM skill fluctuates from minimal values (~0.3) before PCIM to moderate values (~0.5 to 0.6) before PETM until it was high (~0.8 to ~0.9) before both ETM2 and ETM3, and last, reducing to moderate values (~0.4 to 0.5) after ETM3. After ETM3, $\delta^{18}O \rightarrow \delta^{13}C$ keeps rising to ~0.7 for longer library sizes, while $\delta^{13}C \rightarrow \delta^{18}O$ settles to ~0.4, pointing toward an increasing impact of the climate on the carbon cycle.

	Studied time range	Convergence test (CCM skill)	
		$\delta^{13}C \rightarrow \delta^{18}O$	$\delta^{18}O \rightarrow \delta^{13}C$
Before PCIM	61.28–58.068 Ma ago	0.27*	0.29*
Before PETM	58.062–55.935 Ma ago	0.56*	0.51*
Before ETM2	55.141–54.06 Ma ago	0.85*	0.84*
Before ETM3	53.936–52.87 Ma ago	0.87*	0.85*
After ETM3	52.801–48.812 Ma ago	0.38	0.5*

*Within the 95% confidence level.

synchronous causal interaction in both directions. We surmise that this could have made the early Paleogene system particularly sensitive to any external forcing, such as the eccentricity metronome. Previous studies exploring the predictability of the Earth system suggest that a very hot Earth system such as the early Eocene was generally less predictable and, thus, more stochastic than colder climates (*52*, *53*). However, the supporting analyses such as the convergence tests and ECCM undertaken in this study imply that the highly coupled causal skills in both directions observed during EECO could be dynamical in nature, although it is still uncertain whether it is bidirectional or a strongly unidirectional causality (*54*, *55*).

Robustness of the dynamic causality analysis

Recent literature studies on the reliability of the CCM method have pointed out the effect of periodicity/seasonality, autocorrelation, process noise, and trends. These studies show that the absence of causal interaction is much more robust and conclusive than the presence of causal interaction indicated by CCM (*40*, *54*, *55*). Likewise, we performed sensitivity analyses to assess the dependence of the CCM skills in the DCCM analysis on the choice of window size, embedding parameters used for attractor reconstruction, and the type of data transformation such as interpolation, noise reduction, and detrending (see text S3 and figs. S7 to S11 for more details). The dependence of DCCM analysis to these parameters are additionally complicated by the differing effect of these choices on the global carbon cycle and the climate record under study, with the choices affecting the $\delta^{18}O$ record more than the $\delta^{13}C$ record, perhaps because of the lower signal-to-noise ratio. Although the presence of trends can lead to false positives, the question of removing these trends requires additional studies as this can introduce additional artifacts itself. However, the overall trend of the CCM skills in the DCCM analysis and the interpretation of these observations presented in the previous paragraphs are robust and independent of the choice of parameters required to perform the analyses.

In addition, we tested whether our results are critically dependent on the CCM method. Therefore, we reperformed the dynamical causality analysis with an independent method, namely, DRCC (see Materials and Methods and text S4) (*43*, *56*). As shown in Fig. 3C and fig. S12, the RCC skills trends in the DRCC analysis show qualitatively the same trends as the CCM skills in Fig. 3C. The main behavior, such as no causal interactions during PCIM, a higher causal effect of $\delta^{13}C \rightarrow \delta^{18}O$ than $\delta^{18}O \rightarrow \delta^{13}C$ before PETM, and high causal skills during EECO, are consistent between the two methods. Furthermore, fig. S13 shows that the statistical significance of the CCM and RCC skills are robust to the choice of the null model. The DRCC analysis is more robust to noisy data and trends (*43*). Nevertheless, detailed comparisons between DCCM, DRCC, or any other causality analyses on deep time paleo-records are outside the scope of this study. However, with this study, we show how to use causal analyses in deep time paleo-reconstructions and what type of inferences can be extracted from them to better understand the Earth system.

Understanding climate-carbon cycle dynamics

This study indicates that temperature dynamics—as recorded in $\delta^{18}O$—and carbon cycle partitioning—as recorded in $\delta^{13}C$—in the early Eocene Earth system were very strongly coupled and alternated in dominance during this period, concurrent with a long-term decrease in $\delta^{13}C$ values and rise in temperature, although our dataset cannot differentiate between various proposed carbon sources such as methane hydrates (*4*), organic carbon (*49*) in marine sediments, or terrestrial peat deposits (*23*). However, the result in Fig. 3C is consistent with the hypothesis that the climate and the carbon cycle were coupled through an organic carbon capacitor able to store and release carbon on different time scales, having the potential to lead to eventual climate warming (Fig. 1) (*3*, *4*). Our results are consistent with the existence of a capacitor storing extensive amounts of organic carbon during the late Paleocene and early Eocene. A slow release of carbon in tandem with long-term gradual warming toward and through the EECO (*14*) and the tight bidirectional coupling of organic carbon fluxes and the climate system made the Earth system sensitive to carbon release for small initial (orbital) changes, as shown by loss of resilience before the hyperthermal events. The relatively long time scale required to recharge the carbon capacitors together with the higher sensitivity of the hot early Eocene to initial perturbations could explain the overall large magnitude of carbon cycle dynamics. Moreover, the lack of evidence pointing toward ETM3 being climate-driven could be explained by a reduction in size of the carbon capacitor after carbon release for about half a million years.

Our work illustrates the central role of internal amplifying climate-carbon cycle interactions and loss of carbon cycle resilience in triggering late Paleocene–early Eocene global warming events. The timing of most, if not all, hyperthermal events coincides with maxima in orbital eccentricity (*14*, *25*, *41*, *49*), which quantitatively represents only a minor insolation forcing. This requires that dynamical processes such as reinforcing positive feedbacks and loss of stability played a crucial role in these global warming events. Multiplicative noise processes could also have played a role (*53*) and might have increased the susceptibility of the general early Eocene Earth system to the solar insolation. Our results, hence, not only suggest that long-term Paleocene-Eocene warming caused the climate-carbon cycle system to be closer to a threshold (*15*) but also indicate that the whole Earth system became increasingly susceptible to instabilities. In addition, our work provides a new

framework to probe the dynamic causal interaction between two systems. In conclusion, the early Paleogene global warming events are crucial for understanding geologically rapid Earth system changes, including the Anthropocene carbon cycle perturbation and global warming. If the reconstructed early Paleogene dynamics are a characteristic Earth system response, then present-day carbon cycle changes might likewise strengthen positive feedbacks from carbon reservoirs such as permafrost, submarine hydrates, or peatlands. It is therefore critical to constrain the impact of these reservoirs to assess their influence on the magnitude of future global warming.

MATERIALS AND METHODS

High-resolution benthic foraminifer stable isotope record

We used high-resolution records from stratigraphically continuous sections of Late Maastrichtian–early Eocene clayey nannofossil ooze from Ocean Drilling Program sites 1262 and 1263 on the Walvis Ridge in the South Atlantic Ocean. The combined dataset (*16*, *28*) ranging from 67.1 to 48.8 Ma ago comprises 2373 paired deep ocean benthic foraminiferal (*Nuttallides treumpyi*) measurements of stable carbon ($\delta^{13}C$) and oxygen ($\delta^{18}O$) isotope ratios. We used the record from site 1262 for the PETM and ETM2, and the record from site 1263 for ETM3.

Analysis of DIORs

To investigate the change of resilience before the three abrupt global warming events, we used the MATLAB R2019b generic_ews toolbox developed on the basis of (*57*). The DIORs in the form of autoregressive coefficient at lag 1 (AR1) and SD were used to study the loss of resilience in the carbon cycle dynamics and the climate system as the two systems approached each of these three hyperthermal events. Furthermore, we use these DIORs to test the assumption that these abrupt events were possibly tipping points arising because of a zero-eigenvalue bifurcation that can be anticipated by the DIORs (*33*, *35*, *36*, *58*, *59*).

Data curation

The events that we studied are well-defined in the literature as sharp drops in both $\delta^{13}C$ and $\delta^{18}O$ records from the deep ocean benthic foraminifer, and these drops statistically standout beyond the background variability (*60*). We curated a dataset with the same time and data range for both $\delta^{13}C$ and $\delta^{18}O$ records for each of the three described hyperthermal events (PETM, ETM2, and ETM3), and care was taken to exclude the actual hypothesized tipping point and study the DIORs trends in the time series ending just before each hyperthermal event (Table 3). In our figures, the direction of the time range moves from left to right, that is, from older to younger age in million years. For the DIORs analysis, the starting time points for PETM (older age in million years) were selected with the aid of recurrence plots (fig. S14, A and B) (*61*, *62*) to select relatively stationary periods unaffected by other abrupt events (i.e., the Cretaceous-Paleogene boundary and Late Danian event) in both the global carbon cycle and the climate system before the PETM (Table 3). The starting point of the time series before ETM2 was harder to choose. The $\delta^{13}C$ and $\delta^{18}O$ data for ETM2 was curated after the global carbon cycle recovered from the PETM, and ending just before the ETM2 transition, with the understanding that the global carbon cycle takes longer to recover from PETM as it is a much slower system than the climate (*63*). For ETM3, the starting time range was chosen right after ETM2 ended.

DIORs trend and significance test

We detrend the data using a Gaussian filter to remove any trends longer than half a million years for PETM and over 30 ka for ETM2 and ETM3 to prevent spurious changes in autocorrelation because of long-term trends (*57*). For PETM, we focused on processes such as the short and long eccentricity cycles, which occur within half a million years, while we focused on the influence of processes such as precession cycles on the ETM2 and ETM3. DIORs were calculated in a 50% moving window in the curated datasets for each of the three transitions. Autocorrelation was calculated by fitting an AR1 on the moving window, and the trends of each of the indicators were determined by estimating the nonparametric Kendall rank correlation statistic ("Kendall-τ") of the indicators between consecutive windows as the hypothesized transition was approached. The significance of this trend was assessed using 1000 surrogate datasets derived from null models generated by the power spectrum method of Ebisuzaki (*64*). This method creates bootstrapped data having the same power spectra and, in turn, the autocorrelation structure of the original data but with randomized phases to estimate the fraction of these randomized datasets that performed better than the observed dataset (i.e., the *P* value).

Dynamic causality analysis

Convergent cross mapping

CCM is a state space reconstruction (SSR)–based causality analysis that enables to study feedback mechanisms between dynamically related systems by providing directional causal interaction measures. We apply this method to study the interaction between the reconstructions of the global carbon cycle and the climate in the early Paleogene. We assume that the global carbon cycle and the climate are part of a coupled dynamical Earth system, and we thus use attractor reconstruction–based methods to study the interaction of the two systems. Figure S15 gives a schematic

Table 3. Curated dataset. Selected datasets for the DIORs analysis of the three global warming events from the composite record. The same data range was used for the carbon cycle and the climate.

Event	Studied time range	Age range	Average data resolution	Data points	Suspected tipping point	Reference
PETM	61.28–55.935 Ma ago	5.343 Ma	3.82 ka	1397	55.935 Ma ago	(*28*)
ETM2	55.141–54.06 Ma ago	1.081 Ma	2.60 ka	416	54.06 Ma ago	(*28*)
ETM3	53.936–52.87 Ma ago	1.066 Ma	2.59 ka	411	52.87 Ma ago	(*16*)

demonstration of CCM; however, here, we only provide a brief overview of the method and refer to (*39*, *41*, *50*, *65*–*67*) for more detailed descriptions on CCM and state space reconstruction.

The first step of CCM involves SSR based on each of the two time series separately: The reconstructed attractor M_C is based on $\delta^{13}C(t)$ and M_O is based on $\delta^{18}O(t)$. SSR requires choosing a suitable embedding dimension E and time lag-τ (referred to as time lag-τ to avoid confusion with Kendall-τ) (see section S2). These two parameters are interdependent on each other, dependent on the type of data transformation, and the choice of these parameters is also a matter of much debate. Here, we make the choice of time lag-τ = 4 and E = 6 as for E greater than 5 and time lag-τ greater than 3; the SSR and the causality analyses do not depend on the choice of these parameters (figs. S10 and S11).

After SSR, we use weighted simplex projection method to estimate time series, $\hat{O}(t)\,|\,M_C$ and $\hat{C}(t)\,|\,M_O$, based on the nearest neighbors for each point of the time series (leave-one-out cross-validation). Here, $\hat{O}(t)\,|\,M_C$ was the estimated time series of $\delta^{18}O(t)$ based on the reconstructed attractor of $\delta^{13}C(t)$, and $\hat{C}(t)\,|\,M_O$ is the estimated time series of $\delta^{13}C(t)$ based on data of $\delta^{18}O(t)$. The Pearson correlation between $\delta^{13}C(t)$ and $\hat{C}(t)\,|\,M_O$ and between $\delta^{18}O(t)$ and $\hat{O}(t)\,|\,M_C$ was calculated to give the CCM skill (see also fig. S9). The estimation efficiency (CCM skill) of climate based on the carbon cycle dynamics $\hat{O}(t)\,|\,M_C$ could be used as a measure of the causal effect of the climate on the carbon cycle dynamics ($\delta^{18}O \rightarrow \delta^{13}C$), and vice versa, the estimation efficiency of $\hat{C}(t)\,|\,M_O$ is a measure of the causal effect of the carbon cycle on the climate dynamics ($\delta^{13}C \rightarrow \delta^{18}O$). The statistical significance of the CCM skill was calculated using a null model of 100 surrogate time series using power spectrum (*64*) and sieve bootstrap methods (*68*). The sieve bootstrap method generates an AR(n) autoregressive model on the original time series, where the number of lags p was determined on the basis of Akaike information criterion (AIC) criterion. Subsequently, this fitted AR(p) model is used to generate the bootstrapped datasets, drawing replacement from the residuals. Here, we assume that the carbon cycle was causally affecting the climate when the CCM skill of $\delta^{13}C \rightarrow \delta^{18}O$ was within the 95% confidence level, and vice versa.

Convergence test and ECCM analysis

We performed two tests, convergence testing and ECCM analysis, to distinguish causation from spurious correlation (*41*, *50*) on the paired $\delta^{13}C$ and $\delta^{18}O$ records before the PCIM, PETM, ETM2, ETM3, and after ETM3 (see Table 2, Studied time range, and figs. S1 and S2). The convergence test, which is the main part of the CCM analysis (*42*), is used to investigate whether the CCM skill improved with the increasing library size L for determining the nearest neighbors. To test the effect of L, the average CCM skill is determined from all possible overlapping parts of length L of the whole dataset ($L < N$, N is size of whole dataset).

In the case of causation, the CCM skill initially improves with an increase in L eventually converging to a certain CCM skill. In case the time series is predominantly dominated by stochastic noise, the CCM skill does not improve and can sometimes even decrease with increasing library size.

The ECCM analysis was performed to study whether the "cause" preceded the "effect" (*50*). This test was designed to infer whether two-directional highly synchronous dynamics could be due to a common strong external forcing ("confounder") affecting the interacting systems or not. Here, after the first step of SSR, instead of using the nearest neighbors to predict $\hat{O}(t)\,|\,M_C$ from $\delta^{13}C(t)$, the CCM skill was calculated for $\hat{O}(t+d)\,|\,M_C$, with the delay d ranging from −80 to 80 to test past and future values of the time series. If the maximum in the CCM skill occurred for a time delay in the future, then it cannot be assumed to be a real causal link but to be caused because of a strong unidirectional coupling or a common external forcing.

Dynamic convergent cross mapping

We applied CCM in a sliding window approach, here referred to as DCCM, to study the dynamics of changing causal interaction in the climate-carbon cycle system on the $\delta^{13}C$ and $\delta^{18}O$ record from the South Atlantic Ocean, including the hypothesized tipping points between 61.28 and 48.812 Ma ago. This approach allows us to focus on processes and interactions within 1 Ma for each window. The window size was selected to be greater than the library size L at which the CCM skill converges (fig. S1, A to E). Here, the DCCM analysis in Fig. 3 was performed using a window size of 350, maximum library size of 349, time lag-τ of 4, and E as 6, and the window moves by 1 data point. The statistical significance of the CCM skill for each sliding window was calculated using a null model of 1000 surrogate time (*68*). We used the MATLAB ccm toolbox developed on the basis of (*41*) to perform the DCCM analysis. The detailed sensitivity analysis of DCCM to data interpolation (fig. S7A), data noise reduction (fig. S7B), detrending to remove variability over half a million year (fig. S7C), after detrending and noise reduction (fig. S7D), changes in time lag and embedding dimension (figs. S8 and S9), and choice of window size (figs. S10 and S11) are given in text S3.

Dynamic reservoir computing causality

To test the robustness of the DCCM analysis, we modified a recently developed RCC method (*43*, *69*–*70*) to include a sliding window approach, indicated as DRCC. RCC uses a neural network model based on the reservoir computing framework to predict $\delta^{13}C(t)$ from $\delta^{18}O(t)$, and vice versa. Using a dynamic reservoir of N neurons, the algorithm reconstructs the attractor based on the available time series. Similar to DCCM, this method was applied in a moving window of size 350 data points to study the climate-carbon cycle dynamics on the same time scale. The correlation between the reconstructed and original time series is given by the RCC skill. The statistical significance of the RCC skill was calculated using the null models generated by power spectrum and sieve bootstrap method, as was used for the DCCM analysis.

Supplementary Materials

This PDF file includes:

Supplementary Texts S1 to S4
Figs. S1 to S19

REFERENCES AND NOTES

1. T. M. Lenton, H. Held, E. Kriegler, J. W. Hall, W. Lucht, S. Rahmstorf, H. J. Schellnhuber, Tipping elements in the Earth's climate system. *Proc. Natl. Acad. Sci. U.S.A.* **105**, 1786–1793 (2008).
2. R. A. Berner, Z. Kothavala, GEOCARB III: A revised model of atmospheric CO_2 over phanerozoic time. *Am. J. Sci.* **301**, 182–204 (2001).
3. G. Dickens, J. R. O'Neil, D. K. Rea, R. M. Owen, Dissociation of oceanic methane hydrate as a cause of the carbon isotope excursion at the end of the Paleocene. *Paleoceanogr. Paleoclimatol.* **10**, 965–971 (1995).

4. G. R. Dickens, Rethinking the global carbon cycle with a large, dynamic and microbially mediated gas hydrate capacitor. *Earth Planet. Sci. Lett.* **213**, 169–183 (2003).
5. E. A. G. Schuur, A. D. McGuire, C. Schädel, G. Grosse, J. W. Harden, D. J. Hayes, G. Hugelius, C. D. Koven, P. Kuhry, D. M. Lawrence, S. M. Natali, D. Olefeldt, V. E. Romanovsky, K. Schaefer, M. R. Turetsky, C. C. Treat, J. E. Vonk, Climate change and the permafrost carbon feedback. *Nature* **520**, 171–179 (2015).
6. D. Archer, B. Buffett, V. Brovkin, Ocean methane hydrates as a slow tipping point in the global carbon cycle. *Proc. Natl. Acad. Sci. U.S.A.* **106**, 20596–20601 (2008).
7. S. Wieczorek, P. Ashwin, C. M. Luke, P. M. Cox, Excitability in ramped systems: The compost-bomb instability. *Proc. R. Soc. A: Math. Phys. Eng. Sci.* **467**, 1243–1269 (2011).
8. M. Dekker, A. S. von der Heydt, H. Dijkstra, Cascading transitions in the climate system. *Earth Syst. Dynam.* **9**, 1243–1260 (2018).
9. N. Wunderling, J. F. Donges, J. Kurths, R. Winkelmann, Interacting tipping elements increase risk of climate domino effects under global warming. *Earth Syst. Dynam.* **12**, 601–619 (2021).
10. P. U. Clark, J. D. Shakun, S. A. Marcott, A. C. Mix, M. Eby, S. Kulp, A. Levermann, G. A. Milne, P. L. Pfister, B. D. Santer, D. P. Schrag, S. Solomon, T. F. Stocker, B. H. Strauss, A. J. Weaver, R. Winkelmann, D. Archer, E. Bard, A. Goldner, K. Lambeck, R. T. Pierrehumbert, G.-K. Plattner, Consequences of twenty-first century policy for multi-millennial climate and sea-level change. *Nat. Clim. Change* **6**, 360–369 (2016).
11. G. R. Dickens, C. K. Paull, P. Wallace, Direct measurement of in situ methane quantities in a large gas-hydrate reservoir. *Nature* **385**, 426–428 (1997).
12. G. R. Dickens, M. M. Castillo, J. C. G. Walker, A blast of gas in the latest Paleocene: Simulating first-order effects of massive dissociation of oceanic methane hydrate. *Geology* **25**, 259–262 (1997).
13. J. C. Zachos, U. Röhl, S. A. Schellenberg, A. Sluijs, D. A. Hodell, D. C. Kelly, E. Thomas, M. Nicolo, I. Raffi, L. J. Lourens, H. M. Carren, D. Kroon, Paleoclimate: Rapid acidification of the ocean during the paleocene-eocene thermal maximum. *Science* **308**, 1611–1615 (2005).
14. L. J. Lourens, A. Sluijs, D. Kroon, J. C. Zachos, E. Thomas, U. Röhl, J. Bowles, I. Raffi, Astronomical pacing of late Palaeocene to early Eocene global warming events. *Nature* **435**, 1083–1087 (2005).
15. R. E. Zeebe, L. J. Lourens, Solar System chaos and the Paleocene–Eocene boundary age constrained by geology and astronomy. *Science* **365**, 926–929 (2019).
16. V. Lauretano, J. C. Zachos, L. J. Lourens, Orbitally paced carbon and deep-sea temperature changes at the peak of the early Eocene climatic optimum. *Paleoceanogr. Paleoclimatol.* **33**, 1050–1065 (2018).
17. N. Komar, R. E. Zeebe, G. R. Dickens, Understanding long-term carbon cycle trends: The late Paleocene through the early Eocene. *Paleoceanogr. Paleoclimatol.* **28**, 650–662 (2013).
18. D. J. Lunt, A. Ridgwell, A. Sluijs, J. Zachos, S. Hunter, A. Haywood, A model for orbital pacing of methane hydrate destabilization during the Palaeogene. *Nat. Geosci.* **4**, 775–778 (2011).
19. A. Sluijs, P. K. Bijl, S. Schouten, U. Röhl, G.-J. Reichart, H. Brinkhuis, Southern ocean warming, sea level and hydrological change during the Paleocene-Eocene thermal maximum. *Clim. Past* **7**, 47–61 (2011).
20. J. Frieling, F. Peterse, D. J. Lunt, S. M. Bohaty, J. S. Sinninghe Damsté, G.-J. Reichart, A. Sluijs, Widespread warming before and elevated barium burial during the Paleocene-Eocene Thermal Maximum: Evidence for methane hydrate release? *Paleoceanogr. Paleoclimatol.* **34**, 546–566 (2019).
21. S. Kender, K. Bogus, G. K. Pedersen, K. Dybkjær, T. A. Mather, E. Mariani, A. Ridgwell, J. B. Riding, T. Wagner, S. P. Hesselbo, M. J. Leng, Paleocene/Eocene carbon feedbacks triggered by volcanic activity. *Nat. Commun.* **12**, 5186 (2021).
22. T. L. Babila, D. E. Penman, C. D. Standish, M. Doubrawa, T. J. Bralower, M. M. Robinson, J. Self-Trail, R. P. Speijer, P. Stassen, G. L. Foster, J. C. Zachos, Surface ocean warming and acidification driven by rapid carbon release precedes Paleocene-Eocene Thermal Maximum. *Sci. Adv.* **8**, eabg1025 (2022).
23. A. C. Kurtz, L. R. Kump, M. A. Arthur, J. C. Zachos, A. Paytan, Early Cenozoic decoupling of the global carbon and sulfur cycles. *Paleoceanography* **18**, 10.1029/2003PA000908, (2003).
24. R. M. Deconto, S. Galeotti, M. Pagani, D. Tracy, K. Schaefer, T. Zhang, D. Pollard, D. J. Beerling, Past extreme warming events linked to massive carbon release from thawing permafrost. *Nature* **484**, 87–91 (2012).
25. J. Frieling, H. H. Svensen, S. Planke, M. J. Cramwinckel, H. Selnes, A. Sluijs, Thermogenic methane release as a cause for the long duration of the PETM. *Proc. Natl. Acad. Sci. U.S.A.* **113**, 12059–12064 (2016).
26. M. Gutjahr, A. Ridgwell, P. F. Sexton, E. Anagnostou, P. N. Pearson, H. Pälike, R. D. Norris, E. Thomas, G. L. Foster, Very large release of mostly volcanic carbon during the Palaeocene-Eocene Thermal Maximum. *Nature* **548**, 573–577 (2017).
27. T. M. Gernon, R. Barr, J. Godfrey Fitton, T. K. Hincks, D. Keir, J. Longman, A. S. Merdith, R. N. Mitchell, M. R. Palmer, Transient mobilization of subcrustal carbon coincident with Palaeocene–Eocene Thermal Maximum. *Nat. Geosci.* **15**, 573–579 (2022).
28. J. S. K. Barnet, K. Littler, T. Westerhold, D. Kroon, M. J. Leng, I. Bailey, U. Röhl, J. C. Zachos, A high-fidelity benthic stable isotope record of Late Cretaceous–Early Eocene climate change and carbon-cycling. *Paleoceanogr. Paleoclimatol.* **34**, 672–691 (2019).
29. M. J. Cramwinckel, M. Huber, I. J. Kocken, C. Agnini, P. K. Bijl, S. M. Bohaty, J. Frieling, A. Goldner, F. J. Hilgen, E. L. Kip, F. Peterse, R. van der Ploeg, U. Röhl, S. Schouten, A. Sluijs, Synchronous tropical and polar temperature evolution in the Eocene. *Nature* **559**, 382–386 (2018).
30. J. Hansen, M. Sato, G. Russell, P. Kharecha, Climate sensitivity, sea level and atmospheric carbon dioxide. *Philos. Trans. A. Math. Phys. Eng. Sci.* **371**, 20120294 (2013).
31. J. L. Sarmiento, *Ocean Biogeochemical Dynamics* (Princeton Univ. Press, 2013).
32. C. Kuehn, A mathematical framework for critical transitions: Bifurcations, fast–slow systems and stochastic dynamics. *Phys. D* **240**, 1020–1035 (2011).
33. C. Wissel, A universal law of the characteristic return time near thresholds. *Oecologia* **65**, 101–107 (1984).
34. S. Strogatz, Nonlinear dynamics and chaos: With applications to physics, biology, chemistry, and engineering. *Comput. Phys.* **8**, 532 (1994).
35. T. M. Lenton, Environmental tipping points. *Annu. Rev. Environ. Resour.* **38**, 1–29 (2013).
36. E. H. van Nes, B. M. S. Arani, A. Staal, B. van der Bolt, B. M. Flores, S. Bathiany, M. Scheffer, What do tou mean, 'Tipping Point'? *Trends Ecol. Evol.* **31**, 902–904 (2016).
37. U. Feudel, Complex dynamics in multistable systems. *Int. J. Bifurc. Chaos* **18**, 1607–1626 (2008).
38. V. Dakos, M. Scheffer, E. H. van Nes, V. Brovkin, V. Petoukhov, H. Held, Slowing down as an early warning signal for abrupt climate change. *Proc. Natl. Acad. Sci. U.S.A.* **105**, 14308–14312 (2008).
39. G. Sugihara, R. May, H. Ye, C.-h. Hsieh, E. Deyle, M. Fogarty, S. Munch, Detecting causality in complex ecosystems. *Science* **338**, 496–500 (2012).
40. J. Runge, S. Bathiany, E. Bollt, G. Camps-Valls, D. Coumou, E. Deyle, C. Glymour, M. Kretschmer, M. D. Mahecha, J. Muñoz-Marí, E. H. van Nes, J. Peters, R. Quax, M. Reichstein, M. Scheffer, B. Schölkopf, P. Spirtes, G. Sugihara, J. Sun, K. Zhang, J. Zscheischler, Inferring causation from time series in Earth system sciences. *Nat. Commun.* **10**, 2553 (2019).
41. E. H. van Nes, M. Scheffer, V. Brovkin, T. M. Lenton, H. Ye, E. Deyle, G. Sugihara, Causal feedbacks in climate change. *Nat. Clim. Chang.* **5**, 445–448 (2015).
42. E. Weinans, A. W. Omta, G. A. K. van Voorn, E. H. van Nes, A potential feedback loop underlying glacial-interglacial cycles. *Clim. Dynam.* **57**, 523–535 (2021).
43. Y. Huang, Z. Fu, C. L. E. Franzke, Detecting causality from time series in a machine learning framework. *Chaos* **30**, 10.1063/5.0007670, (2020).
44. D. I. Armstrong McKay, T. M. Lenton, Reduced carbon cycle resilience across the Palaeocene-Eocene Thermal Maximum. *Clim. Past Discuss.* **14**, 1515–1527 (2018).
45. C. Boettner, G. Klinghammer, N. Boers, T. Westerhold, N. Marwan, Early-warning signals for Cenozoic climate transitions. *Quat. Sci. Rev.* **270**, 107177 (2021).
46. G. J. Bowen, B. J. Maibauer, M. J. Kraus, U. Röhl, T. Westerhold, A. Steimke, P. D. Gingerich, S. L. Wing, W. C. Clyde, Two massive, rapid releases of carbon during the onset of the Palaeocene-Eocene thermal maximum. *Nat. Geosci.* **8**, 44–47 (2015).
47. V. A. Piedrahita, S. Galeotti, X. Zhao, A. P. Roberts, E. J. Rohling, D. Heslop, F. Florindo, K. M. Grant, L. Rodríguez-Sanz, D. Reghellin, R. E. Zeebe, Orbital phasing of the Paleocene-Eocene Thermal Maximum. *Earth Planet. Sci. Lett.* **598**, 117839 (2022).
48. I. A. van de Leemput, M. Wichers, A. O. J. Cramer, D. Borsboom, F. Tuerlinckx, P. Kuppens, E. H. van Nes, W. Viechtbauer, E. J. Giltay, S. H. Aggen, C. Derom, N. Jacobs, K. S. Kendler, H. L. J. van der Maas, M. C. Neale, F. Peeters, E. Thiery, P. Zachar, M. Scheffer, Critical slowing down as early warning for the onset and termination of depression. *Proc. Natl. Acad. Sci. U.S.A.* **111**, 87–92 (2014).
49. C. J. Hollis, M. J. S. Tayler, B. Andrew, K. W. Taylor, P. Lurcock, P. K. Bijl, D. K. Kulhanek, E. M. Crouch, C. S. Nelson, R. D. Pancost, M. Huber, G. S. Wilson, G. T. Ventura, J. S. Crampton, P. Schiøler, A. Phillips, Organic-rich sedimentation in the South Pacific Ocean associated with late Paleocene climatic cooling. *Earth-Sci. Rev.* **134**, 81–97 (2014).
50. H. Ye, E. R. Deyle, L. J. Gilarranz, G. Sugihara, Distinguishing time-delayed causal interactions using convergent cross mapping. *Sci. Rep.* **5**, 14750 (2015).
51. T. Westerhold, U. Röhl, B. Donner, J. C. Zachos, Global extent of Early Eocene hyperthermal events: A new Pacific benthic foraminiferal isotope record from Shatsky Rise (ODP site 1209). *Paleoceanogr. Paleoclimatol.* **33**, 626–642 (2018).
52. T. Westerhold, N. Marwan, A. J. Drury, D. Liebrand, C. Agnini, E. Anagnostou, J. S. K. Barnet, S. M. Bohaty, D. De Vleeschouwer, F. Florindo, T. Frederichs, D. A. Hodell, A. E. Holbourn, D. Kroon, V. Lauretano, K. Littler, L. J. Lourens, M. Lyle, H. Pälike, U. Röhl, J. Tian, R. H. Wilkens, P. A. Wilson, J. C. Zachos, An astronomically dated record of Earth's climate and its predictability over the last 66 million years. *Science* **369**, 1383–1387 (2020).
53. C. W. Arnscheidt, D. H. Rothman, Asymmetry of extreme Cenozoic climate-carbon cycle events. *Sci. Adv.* **7**, eabg6864 (2021).

54. S. Bartsev, M. Saltykov, P. Belolipetsky, A. Pianykh, Imperfection of the convergent cross-mapping method. *IOP Conf. Ser.: Mater. Sci. Eng.* **1047**, 012081 (2021).
55. S. Cobey, E. B. Baskerville, Limits to causal inference with state-space reconstruction for infectious disease. *PLOS ONE* **11**, e0169050 (2016).
56. Y. Huang, L. Yang, Z. Fu, Reconstructing coupled time series in climate systems using three kinds of machine-learning methods. *Earth Syst. Dynam.* **11**, 835–853 (2020).
57. V. Dakos, S. R. Carpenter, W. A. Brock, A. M. Ellison, V. Guttal, A. R. Ives, S. Kéfi, V. Livina, D. A. Seekell, E. H. van Nes, M. Scheffer, Methods for detecting early warnings of critical transitions in time series illustrated using simulated ecological data. *PLOS ONE* **7**, e41010 (2012).
58. M. Scheffer, J. Bascompte, W. A. Brock, V. Brovkin, S. R. Carpenter, V. Dakos, H. Held, E. H. van Nes, M. Rietkerk, G. Sugihara, Early-warning signals for critical transitions. *Nature* **461**, 53–59 (2009).
59. P. Ashwin, S. Wieczorek, R. Vitolo, P. Cox, Tipping points in open systems: Bifurcation, noise-induced and rate-dependent examples in the climate system. *Philos. Trans. R. Soc., A* **370**, 1166–1184 (2012).
60. S. K. Turner, P. F. Sexton, C. D. Charles, R. D. Norris, Persistence of carbon release events through the peak of early Eocene global warmth. *Nat. Geosci.* **7**, 748–751 (2014).
61. H. Yang, Multiscale recurrence quantification analysis of spatial cardiac vectorcardiogram signals. *IEEE Trans. Biomed. Eng.* **58**, 339–347 (2011).
62. Y. Chen, H. Yang, Multiscale recurrence analysis of long-term nonlinear and nonstationary time series. *Chaos, Solitons Fractals* **45**, 978–987 (2012).
63. R. A. Chisholm, E. Filotas, Critical slowing down as an indicator of transitions in two-species models. *J. Theor. Biol.* **257**, 142–149 (2009).
64. W. Ebisuzaki, A method to estimate the statistical significance of a correlation when the data are serially correlated. *J. Clim.* **10**, 2147–2153 (1997).
65. H. Kantz, T. Schreiber, *Nonlinear Time Series Analysis* (Cambridge Univ. Press, 1997).
66. M. Casdagli, S. Eubank, J. D. Farmer, J. Gibson, State space reconstruction in the presence of noise. *Phys. D* **51**, 52–98 (1991).
67. J. F. Gibson, J. D. Farmer, M. Casdagli, S. Eubank, An analytic approach to practical state space reconstruction. *Phys. D* **57**, 1–30 (1992).
68. P. Bühlmann, Sieve bootstrap for time series. *Bernoulli* **3**, 123–148 (1997).
69. H. Jaeger, Adaptive nonlinear system identification with Echo state networks, in *Proceedings of the 15th International Conference on Neural Information Processing Systems* (MIT Press, 2003), pp. 609–616.
70. H. Jaeger, A tutorial on training recurrent neural networks, covering BPPT, RTRL, EKF and the "echo state network" approach. *ReVision* **2005**, 1–46 (2002).
71. S. Setty, Code used in: Loss of Earth system resilience during Early Eocene transient global warming events. Zenodo. https://doi.org/10.5281/zenodo.7620884.

Acknowledgments: This work heavily relied on decades of work by the International Ocean Discovery Program (IODP) and predecessors, notably the many colleagues who designed the expeditions to recover deep ocean sediments, produced high-resolution age models, and generated the high-resolution isotope records. **Funding:** This work was carried out under the umbrella of the Netherlands Earth System Science Centre (NESSC) and received funding from the European Union's Horizon 2020 research and innovation programme under the Marie Skłodowska-Curie, grant agreement no. 847504. A.S. thanks the European Research Council for Consolidator Grant 771497. **Author contributions:** S.S., M.J.C., E.H.v.N., I.A.v.d.L., M.S., and A.S. designed the study. S.S. carried out the mathematical analyses with the help of E.H.v.N., I.A.v.d.L., and H.A.D. All authors contributed to the interpretation of the results. S.S., M.J.C., E.H.v.N., I.A.v.d.L., H.A.D., and A.S. drafted the paper with input from all the authors. **Competing interests:** The authors declare that they have no competing interests. **Data and materials availability:** All data needed to evaluate the conclusions in the paper are present in the paper and/or the Supplementary Materials. The codes and toolboxes used for the analysis and for creating figures in the paper are freely available on Zenodo (*71*) (https://doi.org/10.5281/zenodo.7620884).

Submitted 23 August 2022
Accepted 6 March 2023
Published 7 April 2023
10.1126/sciadv.ade5466

ScienceAdvances

Loss of Earth system resilience during early Eocene transient global warming events

Shruti Setty, Margot J. Cramwinckel, Egbert H. van Nes, Ingrid A. van de Leemput, Henk A. Dijkstra, Lucas J Lourens, Marten Scheffer, and Appy Sluijs

Sci. Adv., **9** (14), eade5466.
DOI: 10.1126/sciadv.ade5466

Science Advances (ISSN) is published by the American Association for the Advancement of Science. 1200 New York Avenue NW, Washington, DC 20005. The title *Science Advances* is a registered trademark of AAAS.